PNAS RESEARCH ARTICLE | PLANT BIOLOGY

FAB1C, a phosphatidylinositol 3-phosphate 5-kinase, interacts with PIN-FORMEDs and modulates their lytic trafficking in Arabidopsis

Kwang-Ho Maeng[a,1], Hyodong Lee[a,1], and Hyung-Taeg Cho[a,2]

Edited by Mark Estelle, University of California at San Diego, La Jolla, CA; received June 15, 2023; accepted October 10, 2023

PIN-FORMEDs (PINs) are auxin efflux carriers that asymmetrically target the plasma membrane (PM) and are critical for forming local auxin gradients and auxin responses. While the cytoplasmic hydrophilic loop domain of PIN (PIN-HL) is known to include some molecular cues (e.g., phosphorylation) for the modulation of PIN's intracellular trafficking and activity, the complexity of auxin responses suggests that additional regulatory modules may operate in the PIN-HL domain. Here, we have identified and characterized a PIN-HL-interacting protein (PIP) called FORMATION OF APLOID AND BINUCLEATE CELL 1C (FAB1C), a phosphatidylinositol-3-phosphate 5-kinase, which modulates PIN's lytic trafficking. FAB1C directly interacts with PIN-HL and is required for the polarity establishment and vacuolar trafficking of PINs. Unphosphorylated forms of PIN2 interact more readily with FAB1C and are more susceptible to vacuolar lytic trafficking compared to phosphorylated forms. FAB1C also affected lateral root formation by modulating the abundance of periclinally localized PIN1 and auxin maximum in the growing lateral root primordium. These findings suggest that a membrane-lipid modifier can target the cargo-including vesicle by directly interacting with the cargo and modulate its trafficking depending on the cargo's phosphorylation status.

auxin transport | endomembrane trafficking | phosphatidylinositol-3-phosphate 5-kinase | PIN-FORMED (PIN) | FAB1

Auxin functions as a morphogenic hormone by forming local concentration gradients. Auxin efflux carriers, known as PIN-FORMEDs (PINs), contribute to the formation of auxin gradients by localizing asymmetrically at the plasma membrane (PM) and by transporting auxin in a directional, cell-to-cell manner (1, 2). Among the eight PIN members in Arabidopsis, namely PIN1, PIN2, PIN3, PIN4, and PIN7, or the "long PINs" which have a long (~300 a.a.) central hydrophilic loop (HL) domain (3), show diverse and dynamic localization polarities in the PM depending on the PIN member, cell type, developmental stage, and environmental stimuli (4–8).

The HL domain of the long PINs (henceforth referred to as PIN-HL) encompasses a variety of molecular cues that contribute to the intracellular dynamics of PINs. The conserved YXXφ motif, where "X" represents any residue and "X" a large hydrophobic residue, plays a role in clathrin-mediated PIN endocytosis and polarity regulation (9). Additionally, the ubiquitylation of a Lys residue is involved in PIN turnover (10), and various phosphorylation codes in PIN-HL, along with their corresponding kinases, play pivotal roles in determining PIN polarity (2, 11–17) and PIN activity (12, 18–20). The characterization of these molecular cues within PIN-HL has significantly enhanced our understanding of the regulatory mechanisms behind polar auxin transport and auxin responses. However, the wide range of auxin responses observed in various developmental and environmental contexts suggests that PIN-HL likely harbors additional cis- and transregulatory factors that modulate intracellular PIN trafficking and polarity. To identify these potential PIN-modulating factors, we conducted a screening of PIN-HL-interacting proteins (PIPs) and identified FORMATION OF APLOID AND BINUCLEATE CELL 1C (FAB1C), a 1-phosphatidylinositol-3-phosphate 5-kinase that interacts directly with PIN-HL and modulates PIN trafficking to the vacuole.

The dynamic intracellular trafficking of preexisting PINs contributes to their polar localization (21). PIN proteins in the PM follow two trafficking pathways: 1) PM to trans-Golgi network (TGN)/early endosome (EE) to recycling endosome (RE) and back to PM for recycling, or 2) PM to TGN/EE to late endosome (LE)/prevacuolar compartment (PVC)/multivesicular body (MVB) and finally to the vacuole for a lytic pathway (1). While the recycling pathway modulates PIN polarity, the lytic pathway primarily regulates PIN abundance in the PM in response to environmental stimuli and also influences the dynamics of PIN polarity during organogenesis. Under the influence of gravitational

Significance

Phosphatidylinositol kinases are instrumental in endomembrane cargo trafficking by altering local membrane-lipid properties, and PIN-FORMED (PIN) auxin efflux transporters exhibit dynamic intracellular trafficking patterns modulated by the phosphorylation of their hydrophilic loop (HL) domain. Yet, the mechanisms by which phosphatidylinositol kinase establishes the trafficking pathway and selectivity of cargo and how PIN-HL phosphorylation influences PIN trafficking remained enigmatic. This study unveils that FAB1C, a phosphatidylinositol-3-phosphate 5-kinase in Arabidopsis, interfaces directly with PIN-HL, orchestrating PIN's vacuolar trafficking in a PIN-HL phosphorylation-dependent manner. These findings offer a leap forward in deciphering the interplay between membrane-lipid modifiers and cargo selection for endomembrane trafficking and the role of PIN phosphorylation in trafficking, enhancing our understanding of complex eukaryotic cellular processes.

The authors declare no competing interest.

This article is a PNAS Direct Submission.

[1]K.-H.M. and H.L. contributed equally to this work.

[2]To whom correspondence may be addressed. Email: htcho@snu.ac.kr.

This article contains supporting information online at https://www.pnas.org/lookup/suppl/doi:10.1073/pnas.2310126120/-/DCSupplemental.

Published November 7, 2023.

stimuli, the apical PIN2 in the upper epidermal cell undergoes endocytosis and follows a lytic pathway for degradation in the vacuole (22–28). During the development of lateral roots, cytokinin triggers the trafficking of PIN1 for degradation in the vacuole, thereby redirecting its polarity from basal to lateral (29, 30).

Phosphorylated phosphatidylinositol (PtdIns) lipids, located on the cytosolic leaflet of cellular membranes, serve crucial cellular functions, including cytoskeleton organization and membrane trafficking (31–33). Changes in the phosphorylation status of the inositol ring of a PtdIns closely correlate with membrane trafficking dynamics (34, 35). Phosphatidylinositol 3,5-bisphosphate (PtdIns(3,5)P_2), synthesized from PtdIns(3)P by PtdIns(3)P5-kinase (known as FAB1 in plants, Fab1p in yeast, and PIKfyve in mammals), participates in vacuolar homeostasis, autophagy regulation, and endosomal trafficking (31, 33, 36). Arabidopsis possesses four FAB1 homologs (FAB1A to D), where FAB1A and FAB1B are canonical with the FYVE domain necessary to recognize PtdIns(3)P. In contrast, FAB1C and FAB1D lack this typical FYVE domain (33, 37, 38). Research using mutants, artificial microRNA, and FAB1 inhibitors suggests that plant FAB1s have cellular roles in vacuolar organization and acidification (38, 39) and membrane- or cargo-trafficking processes (40–42). Some of these studies indicate that FAB1 plays a role in the lytic trafficking of PM cargos, including PIN2 and BOR1 (HIGH BORON 1) in Arabidopsis (41, 42). However, how FAB1 influences the lytic trafficking of cargo in eukaryotes remains to be understood. In this context, we demonstrate that Arabidopsis FAB1C interacts directly with PIN cargos to guide them to lytic trafficking in a cargo phosphorylation-dependent manner.

Results

FAB1C Interacts Directly with PIN-HL In Vitro and In Planta. FAB1C was identified as a PIN interactor through protein pulldown from the protein extract of Arabidopsis seedlings using the PIN3-HL domain as bait, followed by mass spectrometry analysis (43). The FAB1C protein, starting from the N terminus, comprises a FYVE-like domain (FVL), a PIN-interacting domain (PD, identified in this study), a T-complex1 domain (TCP), a conserved Cys-rich domain (CCR), and a PtdIns-kinase domain (PIK) (Fig. 1*A* and *SI Appendix*, Fig. S1*A*). Despite the FVL domain of FAB1C showing overall low homology with the FYVE domain of canonical FAB1s, such as FAB1A and FAB1B, the structurally significant Cys residues and their intervals appear to be conserved in FAB1C's FVL domain as well (*SI Appendix*, Fig. S1*A*).

To confirm the physical interaction between FAB1C and PIN-HL and to identify the specific region of FAB1C that interacts with PIN, we conducted yeast two-hybrid (Y2H) and in vitro protein pulldown assays using various domain fragments of FAB1C and HLs from PIN1, PIN2, and PIN3 (Fig. 1 *A* and *B*). In yeast cells, the full-length FAB1C sequence interacted with all HL domains from PIN1, PIN2, and PIN3, indicating that FAB1C might be a general interactor with long PINs. Y2H assays, involving sequential domain deletion of FAB1C, revealed that the PIN-interacting domain (PD) was crucial for interaction with PIN-HLs and was sufficient on its own to interact with them. However, the weakened interaction between the C-terminal-deleted FAB1C and PIN2- and PIN3-HL suggested that the C-terminal region might also contribute to the interaction. In the in vitro protein pulldown assays, the N-terminal region, including PD, interacted with all HLs from PIN1, PIN2, and PIN3, while the middle and C-terminal regions did not. Conversely, PD alone displayed a clear interaction with PIN2-HL but showed weak or no interaction with PIN1- and PIN3-HL in the pulldown assay. These Y2H and in vitro interaction results suggest that while the PD region of FAB1C likely plays a key role in interacting with PIN-HLs, other regions at the N or C terminus of FAB1C might also contribute to this interaction. The AlphaFold-predicted model of the PD region did not represent a distinctive three-dimensional structure, indicative of certain flexibility in protein interactions (*SI Appendix*, Fig. S1 *B* and *C*).

We sought to identify the region of PIN2-HL that primarily interacts with FAB1C-PD. We divided PIN2-HL into three regions (HL1, 2, and 3; Fig. 1*C* and *SI Appendix*, Fig. S2) and examined their interactions with PD using an in vitro protein pulldown assay. The assay revealed that PD predominantly interacts with the HL3 region of PIN2-HL (Fig. 1*C*).

Given the previous implications of FAB1A and FAB1B in PIN2 trafficking (41), we investigated whether the corresponding PD regions of FAB1A and FAB1B also interact with PIN-HL. In in vitro pulldown assays, both FAB1A-PD and FAB1B-PD exhibited clear interaction with PIN2-HL, but they showed weak or no interaction with the HL of PIN1 and PIN3 (Fig. 1*D*), mirroring the interaction observed with FAB1C-PD (Fig. 1*B*). This finding suggests that the PD region in FAB1 homologs may generally interact with PIN2-HL, at the very least.

We evaluated the in vivo interaction between FAB1C and PIN2 using Förster Resonance Energy Transfer by Fluorescence Lifetime Imaging (FRET-FLIM) analysis. This was conducted with a cotransgenic plant expressing both the FAB1C promoter:FAB1C:reporter fusion [*ProFAB1C:FAB1C:RFP* (Red Fluorescent Protein)] and PIN2 promoter:PIN2:reporter fusion [*ProPIN2:PIN2:GFP* (Green Fluorescent Protein)] constructs. To also test whether the PIN-interacting domain and the PIK activity of FAB1C are necessary for this in vivo interaction, we generated truncated FAB1C in PD (ΔPD) or PIK (ΔPIK) and point-mutated FAB1C in the catalytic residue of PIK (mPIK). In yeast FAB1, PIK activity was entirely eliminated by a point mutation of the catalytic residue (D2134R) (44), which is also strictly conserved in FAB1 homologs of animals and green plant lineages, including Arabidopsis FAB1s (*SI Appendix*, Fig. S3*A*). We made a point mutation in FAB1C at this residue (D1508R; namely, mPIK). These FAB1C mutant forms and wild type (WT)-FAB1C under its own promoter were introduced into the *fab1c* mutant. The mutated FAB1C forms displayed a similar subcellular localization pattern, and the lines used for FRET-FLIM analysis showed a similar expression level to those of WT-FAB1C in terms of RFP intensity (Fig. 1*G* and *SI Appendix*, Fig. S3*B*). The fluorescence lifetime of PIN2:GFP significantly decreased in the WT-FAB1C:RFP and PIN2:GFP double transgenic plant compared to the PIN2:GFP single transgenic plant in the analysis with the region of interest (ROI) taken from the whole root-meristem area (Fig. 1 *E* and *F* and *SI Appendix*, Fig. S3*D*). This indicates that the resonance energy from PIN2:GFP was transferred to WT-FAB1C:RFP, suggesting a physical interaction between the two proteins in vivo. To obtain more detailed information about the subcellular location of the interaction between PIN2 and FAB1C, we conducted a further FRET-FLIM analysis using subcellular ROIs from both the PM and intracellular areas (*SI Appendix*, Fig. S3 *C* and *D*). A significant reduction in the PIN2:GFP lifetime was observed solely in the intracellular ROI (*SI Appendix*, Fig. S3*C*). As FAB1C exhibited no PM-localization pattern and instead displayed a cytoplasmic distribution (Fig. 1 *E* and *G* and *SI Appendix*, Fig. S4), and considering a portion of PIN2 is believed to undergo intracellular trafficking, it is likely that the reduction in the PIN2:GFP lifetime originated from the cytoplasmic region. In contrast to the result with WT-FAB1C, the deletion of PD eliminated the interaction with PIN2, whereas the deletion or point mutation of PIK of FAB1C did not significantly impact the interaction (Fig. 1*F*).

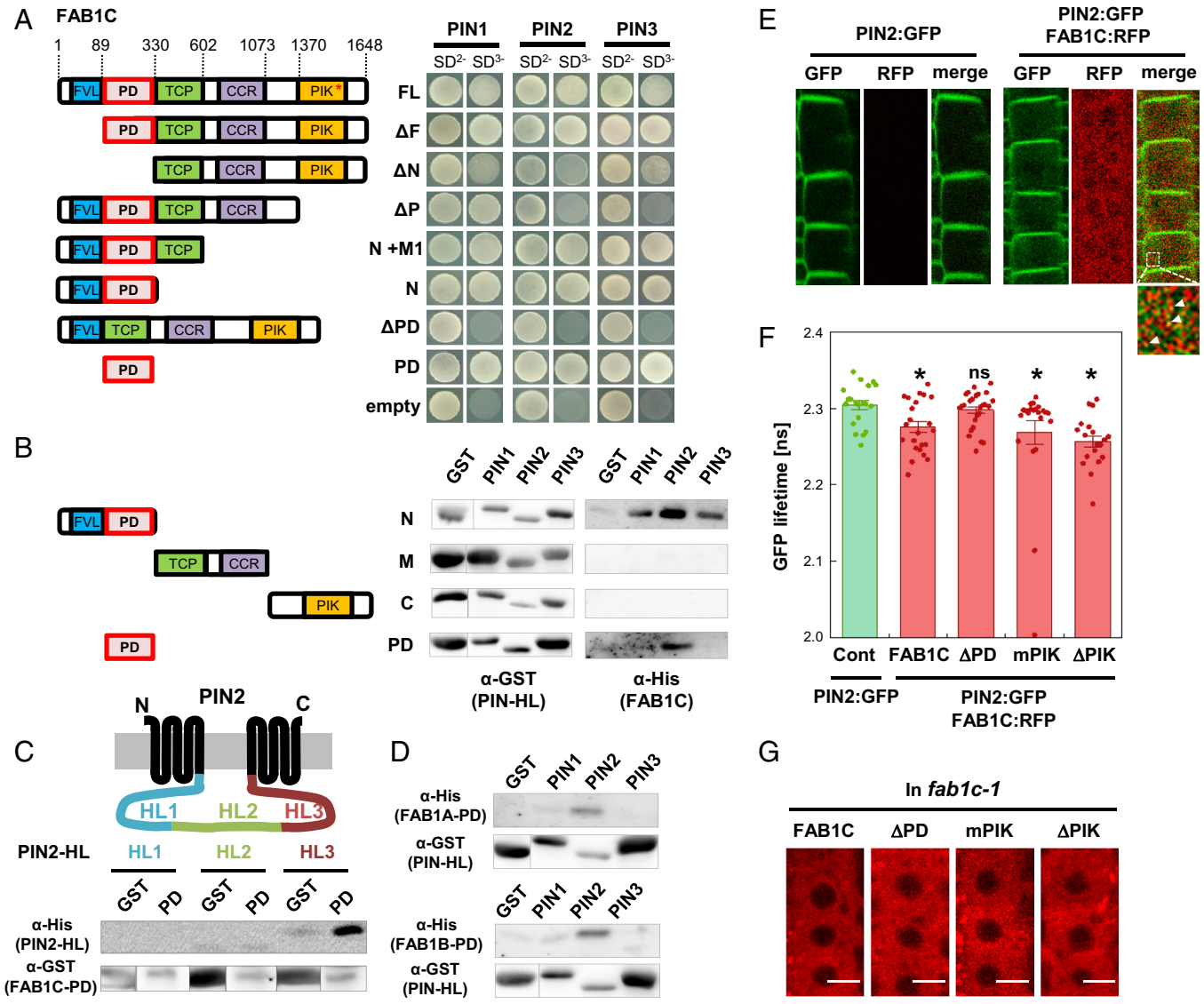

Fig. 1. FAB1C directly interacts with PIN-HL in vitro and in vivo. (*A*) Schematic domain structures of FAB1C and yeast two-hybrid assays showing the interaction between FAB1C and PIN-HL. FVL, FYVE-like; PD, PIN-interacting domain; TCP, T-complex1; CCR, conserved cystein rich; PIK, phosphoinositide kinase; FL, full length; N, N terminus; C, C terminus; M1, middle region 1; M2, middle region 2; SD^{2-}, (-Leu/-Trp); SD^{3-}, (-Leu/-Trp/-His). (*B*) In vitro pulldown assays demonstrating the interaction between FAB1C fragments and PIN-HL. Immunoblot analyses were conducted for GST:PINs-HL (with aniti [α]-GST antibody) or for His:FAB1C fragments (with α-His antibody) after pulldown of them with each PIN-HL. (*C*) In vitro pull-down assays for the interaction between PD and three PIN2-HL fragments. Immunoblot analyses were conducted for GST:FAB1C-PD or for His:PIN2-HL1~3 fragments after its pulldown with GST:FAB1C-PD. (*D*) In vitro pulldown assays showing the interaction between PIN-HL and PD of FAB1 homologs (FAB1A and FAB1B). Immunoblot analyses were conducted for GST:PIN-HL or for His:FAB1-PD after its pulldown with each GST:PIN-HL. Representative data from three independent experiments with similar results are presented in *A*–*D*. (*E* and *F*) FRET-FLIM analysis showing the in vivo interaction between PIN2 and FAB1C in root epidermal cells. Arrowheads indicate colocalization between FAB1C and PIN2 in the cytoplasm (*E*). GFP lifetimes of the *ProPIN2:PIN2:GFP* single transformant (Cont) and the *ProPIN2:PIN2:GFP* × *ProFAB1C:FAB1C:RFP* (FAB1C, intact; ΔPD, deleted PD; mPIK, point-mutated in PIK as denoted by asterisk (*A*); ΔPIK, deleted PIK domain) double transformant were quantitatively compared (*F*). Data represent mean ± SE [n = 19 to 26 ROIs from the whole root-meristem area; Significant difference to the Cont value was denoted by * ($P < 0.05$, Student's *t* test; ns, not significant)]. (*G*) Subcellular localization of intact or mutated FAB1C as seen in *F*. (Bar, 10 μm.)

These results suggest that while the PtdIns-kinase activity is not involved, the PD of FAB1C is necessary for its interaction with PIN2 in vivo.

FAB1C Is Mainly Localized to the Cytoplasm. We examined the expression pattern of the *FAB1C*-transcriptional marker and the FAB1C protein in the root and leaf using *ProFAB1C:GUS* (*β-Glucuronidase*) and *ProFAB1C:FAB1C:GFP*, respectively. *FAB1C* was expressed in most cell types at the root tip and was mainly confined to the vascular tissues in mature root regions (*SI Appendix*, Fig. S4 *A* and *B*). Also, *FAB1C* expression was prominent in the lateral root primordium throughout all its developmental stages (*SI Appendix*, Fig. S4 *A* and *C*). In leaf tissues, *FAB1C* was expressed in veins and strongly in the hydathode (*SI Appendix*, Fig. S4*A*).

When it comes to its location within cells, the FAB1C:GFP fusion protein in root cells was found throughout the cytoplasm (*SI Appendix*, Fig. S4 *B* and *C*). This subcellular localization pattern of FAB1C is similar to that of FAB1D (45), but distinctive from those of FAB1A and FAB1B, which are localized to LE, PM, endoplasmic reticulum (ER), and vacuole depending on the cell type (41, 46). This distinctive subcellular localization between canonical and noncanonical FAB1s could be due to the presence or absence of the FYVE domain, which is required to bind PtdIns(3)P on the cellular membranes (33, 36, 47).

FAB1C Is Required for the Proper Trafficking of PINs. The physical interaction between FAB1C and PIN-HL led us to investigate whether FAB1C impacts the intracellular trafficking of PIN proteins. We introduced *PIN1:GFP, PIN2:GFP*, and *PIN3:GFP* fusion constructs into loss-of-function *fab1c* mutant backgrounds (*fab1c-1* and *fab1c-3*; *SI Appendix*, Fig. S5) and observed changes in the subcellular localization of PIN1, 2, and 3. Two noticeable common features in PIN trafficking under FAB1C deficiency were the accumulation of vesicles containing PIN proteins and partial disruption of their polarity in the PM. In *fab1c* mutants, PIN1 and PIN3 accumulated into relatively large intracellular vesicles in root vascular cells, while PIN2 accumulated into smaller vesicles in root epidermal cells (Fig. 2 *A*, *B*, *D*, *E*, *K*, and *L* and *SI Appendix*, Fig. S6 *A*, *B*, and *D*–*G*). Restoring FAB1C expression by introducing *ProFAB1C:FAB1C:RFP* in the *fab1c* mutant reinstated the wild-type level of intracellular PIN2 vesicles (Fig. 2 *D* and *E*).

Furthermore, the basal polarity of PIN1 in root vasculature, apical polarity of PIN2 in root epidermis, and lateral polarity of PIN3 in root pericycle were all compromised in *fab1c* mutants when compared to WT (Fig. 2 *C*, *H*, and *M* and *SI Appendix*, Fig. S6 *C* and *H*). In root meristematic cortical cells, the loss of FAB1C significantly increased the shootward (apical) PIN2 polarity (Fig. 2 *I* and *J*), which is similar to the previous observation where gene suppression by artificial microRNA of *FAB1A*/*B* or FAB1 inhibitor treatment caused PIN2 polarity changes from rootward to shootward in the same cell type (41). In regard to the partial disruption of apical PIN2 polarity in root epidermal cells, we examined whether it was related to the levels of PIN2 in the PM. Our analysis revealed no significant correlation between the degree of apical PIN2 polarity and PIN2 levels (*SI Appendix*, Fig. S7), suggesting that the compromised PIN2 polarity in the *fab1c* mutant resulted from changes other than in the PIN2 protein level.

Another phenotypic effect of the loss of *FAB1C* was the increase in PIN2 (and also PIN1, as will be discussed later) protein levels in the PM (Fig. 2*F*), despite no clear increase in *PIN2* transcript levels in the *fab1c* mutant (*SI Appendix*, Fig. S8*A*). This finding suggests that FAB1C may play a role in the vacuolar trafficking of PIN. To explore this possibility, we used the endocytic tracer dye FM4-64 to track PIN2:GFP, considering that the PIN2-containing internal vesicles in *fab1c* could be part of the lytic pathway. FM4-64 stains the PM and then undergoes sequential endocytic processes to the vacuole via EE and LE (48). FM4-64 reaches EE in 6 to 15 min, LE in 30 to 60 min, and vacuolar tonoplast in 90 to 120 min after its application (49, 50, 51). We chose 10- and 45-min time points after FM4-64 application to distinguish between EE- and LE-enriched vesicles. Most (86 to 94%) of the internal PIN2 signals in the *fab1c* mutant colocalized with endocytosed FM4-64, which represented either EE- or LE-enriched vesicles (Fig. 2*N* and *SI Appendix*, Fig. S6*I*). The most noticeable observation was a significant increase in EE-enriched vesicles containing PIN2 in the *fab1c* mutant. The number of PIN2-containing EE-vesicles was 2.46-fold higher in the mutant than in WT (Fig. 2*O* and *SI Appendix*, Fig. S6*I*). Meanwhile, the number of LE-vesicles showed a 1.41-fold increase in the mutant compared to WT. This increased accumulation of PIN2-containing EE and LE in the *fab1c* mutant suggests that FAB1C is necessary for PIN2 trafficking from EE onward.

FAB1C Promotes Vacuolar Trafficking of PIN2. The increased intensity of PIN2 at the PM and the higher localization of PIN2 in EE and LE in the *fab1c* mutant compared to WT prompted us to test whether FAB1C positively influences the vacuolar trafficking of PIN2. To do this, we first examined the relationship between PIN2 signal intensity at the PM and FAB1C signal intensity in the cytoplasm of root epidermal cells. We introduced a construct expressing FAB1C (*Pro35S:FAB1C:RFP*) into a transformant containing *ProPIN2:PIN2:GFP* and obtained independent lines that express different levels of FAB1C:RFP. There were no significant differences in *PIN2* transcript levels across different lines expressing varying levels of FAB1C:RFP (Fig. 3 *A* and *B* and *SI Appendix*, Fig. S8*B*). When we examined the correlation between intensities of PIN2:GFP and FAB1C:RFP proteins in the same root, PIN2 signal intensity decreased proportionally with increasing FAB1C intensity (Fig. 3*B*). This suggests that FAB1C could be involved in the lytic process of PIN2 protein, which is reminiscent of the previous observation that the *FAB1A*/*FAB1B* cosuppression interfered with PIN2 degradation at the upper epidermis of gravi-stimulated root (41).

Previous studies have shown that the vacuolar targeting of GFP-tagged PIN2 is observable under dark conditions (24, 52), and that cytokinin induces vacuolar degradation of PIN1 during lateral root development (29, 30). We utilized these vacuolar trafficking-indicating systems to further explore the role of FAB1C in the vacuolar trafficking of PIN2. Compared to WT, the *fab1c* mutant displayed delayed vacuolar accumulation of PIN2 under darkness (Fig. 3 *C* and *D*). Furthermore, benzyladenine (BA, a synthetic cytokinin) treatment led to vacuolar accumulation of PIN1 in lateral root primordia cells of WT, but this was almost completely eliminated in the *fab1c* mutant (Fig. 3 *E* and *F*). These findings suggest that FAB1C plays a significant role in the vacuolar trafficking of PINs.

PIN-Interacting Domain and PtdIns-Kinase Activity Are Required for FAB1C-Mediated Vacuolar Trafficking of PIN2. Considering the observations that FAB1C plays a role in the vacuolar trafficking of PINs, we evaluated the molecular function of two FAB1C domains during the vacuolar accumulation of PIN2 under the dark. These two domains include the PD of FAB1C, which has been shown to play a major role in interacting with PINs both in vitro and in vivo (Fig. 1), and the PIK domain, which is known to be the catalytic moiety for FAB1 to produce $PI(3,5)P_2$ (36, 39). To assess whether the PD-mediated interaction with PIN and the PIK activity is crucial for the vacuolar PIN trafficking, we observed the vacuolar PIN2 accumulation under darkness in the *fab1c* mutant line complemented with WT-FAB1C or mutated FAB1C forms in the PD and PIK domain (ΔPD, ΔPIK, and mPIK as seen in Fig. 1*F*). In the complementation experiment, while WT-FAB1C successfully restored the vacuolar accumulation of PIN2 in the *fab1c* mutant background, the mutated FAB1Cs in the PD or PIK domain failed to restore the FAB1C function (Fig. 3 *G* and *H*).

Given that FAB1C influenced PIN polarity, we also evaluated whether the intact PD and PIK domains in FAB1C are necessary for normal PIN2 polarity in root epidermal cells. When introduced into the *fab1c* mutant, WT-FAB1C restored the WT level of apical PIN2 polarity. In contrast, ΔPD, ΔPIK, and mPIK forms of FAB1C failed to restore the polarity (*SI Appendix*, Fig. S9 *A* and *B*).

These results suggest that both the interaction with PIN2 via PD and the production of $PtdIns(3,5)P_2$ via the intact PIK domain are essential for FAB1C to mediate the vacuolar trafficking of PIN2.

Unphosphorylated PIN2 Forms Are Preferred for Vacuolar Trafficking. PIN-HL contains multiple phosphorylation sites that are key in regulating intracellular PIN trafficking and PIN activity (43, 53). However, how the phosphorylation status of PIN-HL modulates PIN trafficking remains unclear. Therefore, we investigated whether the phosphorylation status of those residues

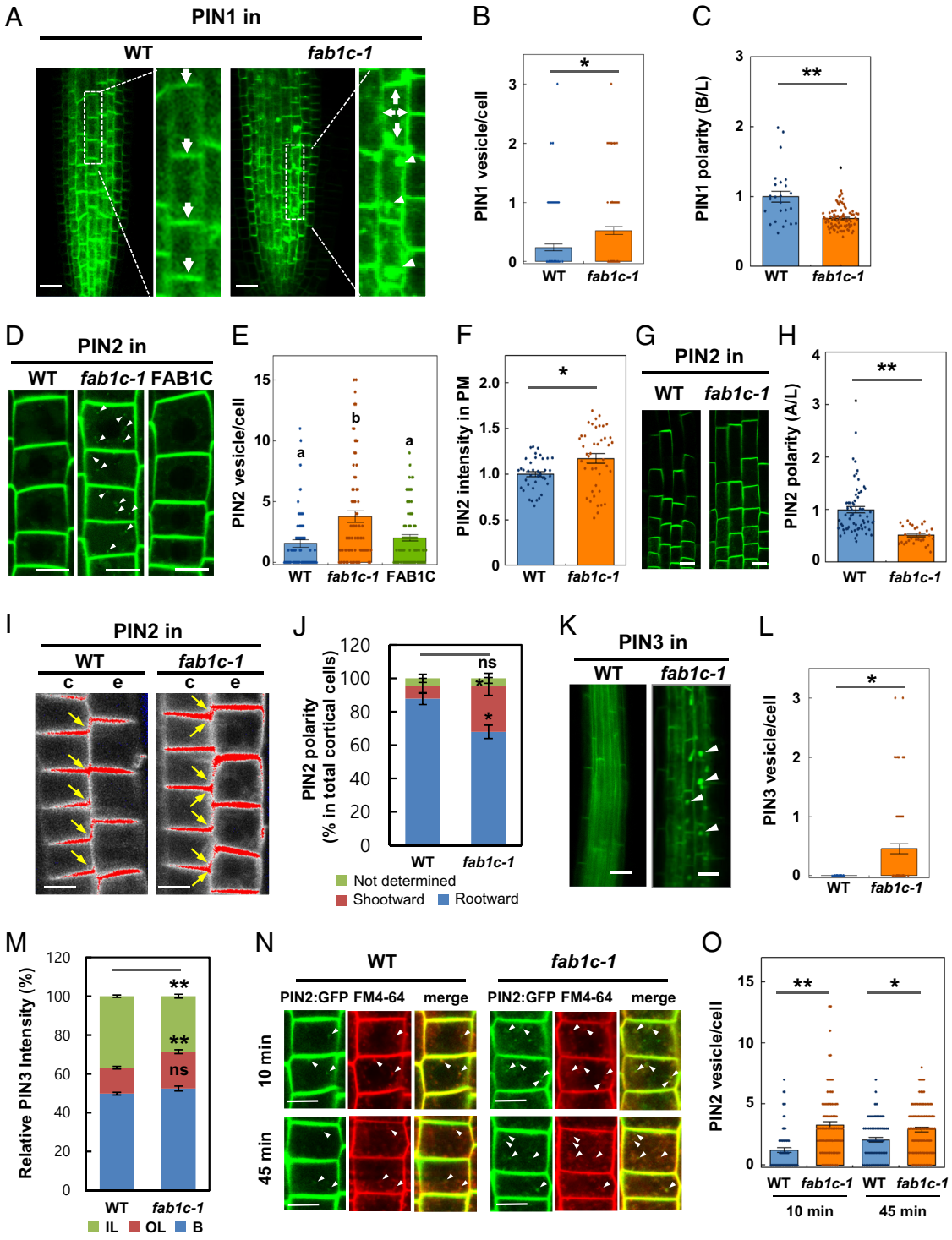

Fig. 2. The *FAB1C* loss-of-function alters PINs trafficking and polarity. (*A–C*) Altered PIN1 (*ProPIN1:PIN1:GFP*) trafficking in the vascular cells of *fab1c* mutant. (*A*) Confocal images of subcellular PIN1 localization. Internalized PIN1 vesicles were observed in 5 out of 13 PIN1-transgenic lines in the *fab1c-1* mutant while none was observed in wild type (WT). (Bar, 20 μm.) Arrows and arrowheads indicate PIN1 polarity and internal vesicles, respectively. (*B*) The number of PIN1-including internal vesicles. (*C*) The relative ratio of basal/lateral (B/L) polarity of PIN1 [n = 100 to 120 cells from 10 to 12 seedlings (*B*) and 25 to 85 cells from 5 to 17 seedlings (*C*)]. (*D–J*) Alteration of PIN2 (*ProPIN2:PIN2:GFP*) trafficking in the root epidermal (*D–H*) and cortical (*I* and *J*) cells of *fab1c* mutant. (*D*) Confocal images of subcellular PIN2 localization in the root epidermis in WT, *fab1c-1* mutant, and *fab1c-1* mutant complemented with FAB1C (*ProFAB1C:FAB1C:RFP*). Internal PIN2 vesicles are indicated by arrowheads. (Bar, 10 μm.) (*E*) The number of PIN2-including internal vesicles seen in *D* [n = 65 to 88 cells from 13 to 18 seedlings; Significant differences are denoted by different letters (ANOVA test, $P < 0.05$)]. (*F*) The relative intensity of PIN2 signal in the PM seen in *D* (n = 39 to 46 cells from 9 to 11 seedlings). (*G*) Confocal images of PIN2 signals in the epidermis of upper root meristematic zone. (Bar, 10 μm.) (*H*) The relative ratio of apical/lateral (A/L) PIN2 polarity seen in *G* (n = 29 to 64 cells from 5 to 13 seedlings). (*I*) Confocal images of PIN2 signal in cortical (c) and epidermal (e) cells. Arrows indicate PIN2 polarity. (Bar, 10 μm.) (*J*) The ratio of PIN2 polarity among the observed total cortical cells shown in *I* (n = 28 to 41 cells from 5 to 7 seedlings; ns, not significant). (*K–M*) Altered PIN3 (*ProPIN3:PIN3:GFP*) trafficking in the vascular cells of *fab1c* mutant. (*K*) Confocal images of subcellular PIN3 localization. (Bar, 20 μm.) Arrowheads indicate PIN3-including internal vesicles. (*L*) The number of PIN2-including internal vesicles seen in *K*. (*M*) Relative intensity of PIN3 signal in the inner lateral (IL), outer lateral (OL), and basal (B) PM of pericycle cells [n = 45 to 90 cells from 9 to 18 seedlings (*L*) and 40 to 48 cells from 8 to 10 seedlings (*M*)]. (*N* and *O*) Colocalization of FM4-64 and PIN2 (*ProPIN2:PIN2:GFP*) in root epidermal cells. (*N*) Confocal images of PIN2-expressing epidermal cells stained with FM4-64 for given time periods. Arrowheads indicate colocalized PIN2:GFP vesicles with FM4-64. (Bar, 10 μm.) (*O*) The number colocalized PIN2:GFP vesicles with FM4-64 seen in *N* (n = 68 to 101 cells from 12 to 19 seedlings). Data represent mean ± SE (Student's *t* test, $*P < 0.05$ and $**P < 0.0001$; *B*, *C*, *E*, *F*, *H*, *J*, *L*, *M*, and *O*).

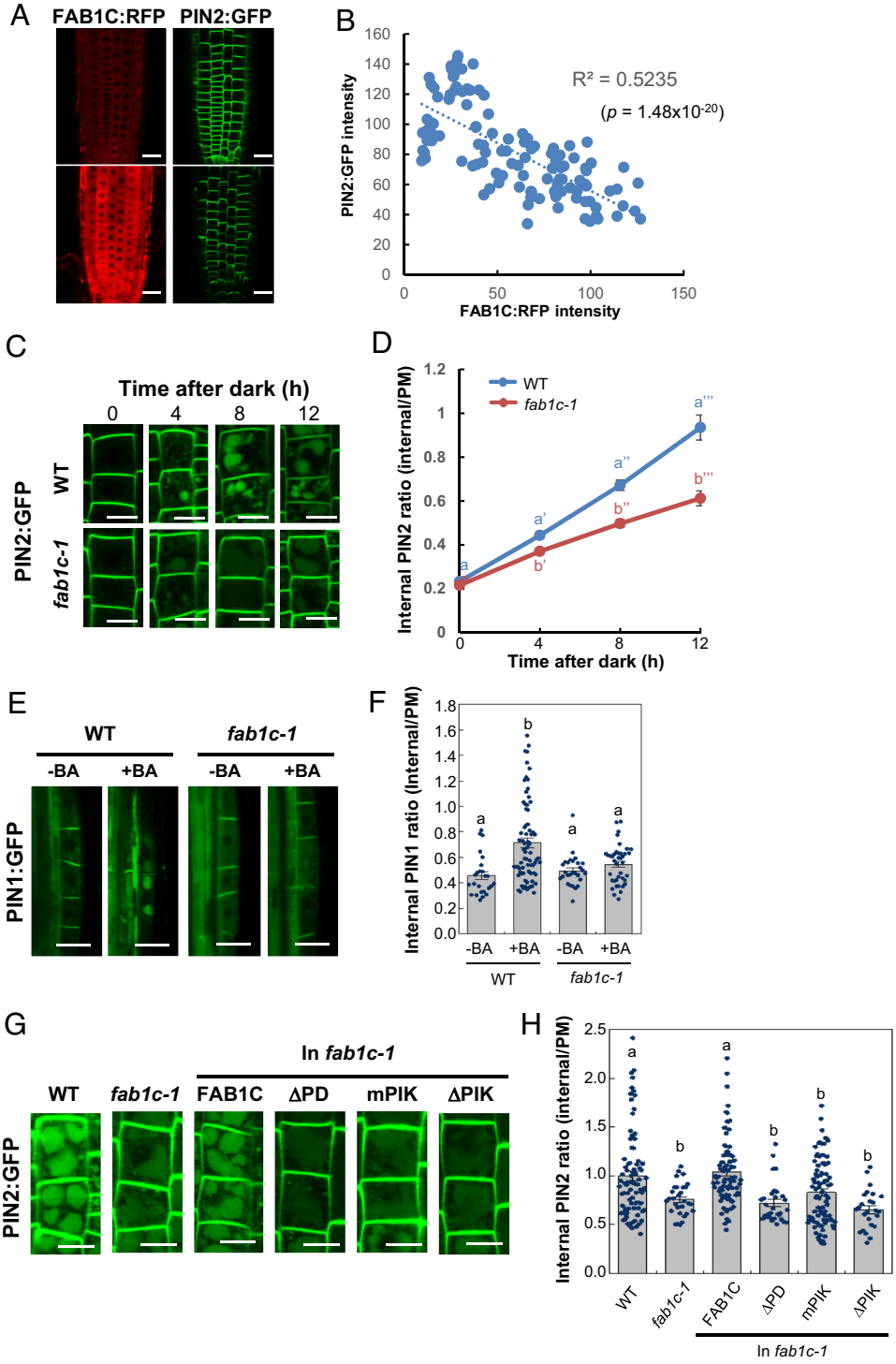

Fig. 3. FAB1C is required for the vacuolar trafficking of PINs. (*A*) Representative confocal images showing fluorescence signals of FAB1C:RFP and PIN2:GFP in the root epidermis of the double transgenic *Pro35S:FAB1C:RFP* × *ProPIN2:PIN2:GFP* plants. (Bar, 20 μm.) (*B*) The relationship between PIN2:GFP intensity and FAB1C:RFP intensity from the double transgenic in *A*. R^2 denotes Pearson's correlation coefficient (n = 119 cells from 12 seedlings). (*C*) Dark-induced vacuolar trafficking of PIN2 in WT and *fab1c-1* mutant. PIN2:GFP signals in the root epidermis were observed after incubation in the dark. (Bar, 10 μm.) (*D*) The signal intensity ratio of internalized vs. PM-localized PIN2:GFP after dark treatment as shown in *C* (n = 30 to 110 cells from 3 to 11 seedlings). (*E*) Representative images showing cytokinin (BA)-induced vacuolar trafficking of PIN1 (*ProPIN1:PIN1:GFP*) in the lateral root primordia of WT and *fab1c-1* mutant. (Bar, 10 μm.) (*F*) The signal intensity ratio of internalized vs. PM PIN1:GFP in the lateral root primordia as shown in *E* (n = 25 to 75 cells from 4 to 9 seedlings). (*G*) Dark-induced vacuolar trafficking of PIN2 in WT, *fab1c-1*, and the *fab1c-1* mutant complemented with intact or mutated FAB1C (*ProFAB1C:FAB1C:RFP*, as described in Fig. 1*F*). PIN2:GFP (*ProPIN2:PIN2:GFP*) was observed 8 h after dark treatment. (Bar, 10 μm.) (*H*) The signal intensity ratio of internalized vs. PM PIN2:GFP as shown in *G* (n = 25 to 90 cells from 5 to 18 seedlings). Data represent mean ± SE, and different letters indicate significant differences (one-way ANOVA with Tukey's unequal N-HSD post hoc test, $P < 0.05$; *D*, *F*, and *H*).

in PIN-HL affects the interaction with FAB1C and its homologs. We selected several representative phosphorylation sites—S1~3 (S237/258/310), S5 (S222), and M3 (S209/S222/T227/S237)—of PIN2-HL (12–15, 54, 55 and *SI Appendix*, Fig. S2) and generated their phospho-defective and phospho-mimetic versions. We then tested their interaction with the FAB1C-N fragment in in vitro

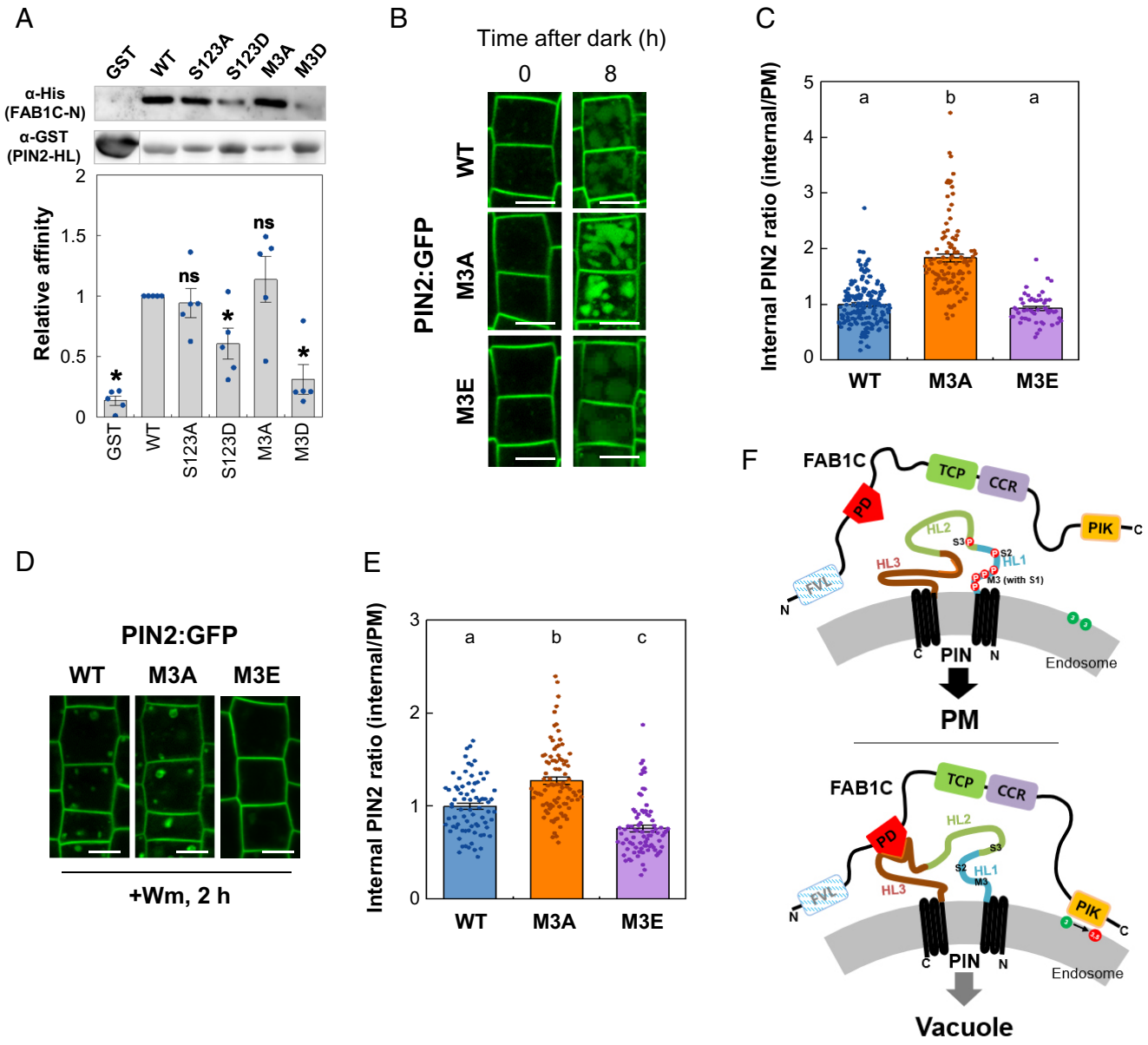

Fig. 4. Unphosphorylated PIN2 forms more preferably interact with FAB1C and are more prone to the lytic process than phosphorylated forms. (*A*) Immunoblot analysis of His:FAB1C-N after its pulldown with phospho-defective/mimetic forms of GST:PIN2-HL (M3A or D, S209/212/215/T227/S231A or D; phospho-sites as shown in *SI Appendix*, Fig. S2). FAB1C-N levels after pulldown, as shown in the bar graph, were normalized with each PIN2-HL level. Data represent means ± SE from five independent assays. Significant differences from the WT value were denoted by * ($P < 0.05$, Student's *t* test; ns, not significant). (*B* and *C*) Dark-induced vacuolar trafficking of wild-type PIN2 (*ProPIN2:PIN2:GFP*, WT), phospho-defective PIN2 (*ProPIN2:M3APIN2:GFP*, M3A), and phospho-mimetic PIN2 (*ProPIN2:M3EPIN2:GFP*, M3E). PIN2:GFP signals in the root epidermis were observed 8 h after incubation in the dark. Bar, 10 μm (*B*). (*C*) Signal intensity ratios of internalized vs. PM PIN2:GFP after dark treatment as shown in *B* (n = 50 to 165 cells from 10 to 33 seedlings). Data represent mean ± SE. (*D* and *E*) Wortmannin (Wm) effect on internalization of different PIN2 forms. PIN2:GFP signals in the root epidermis were observed 2 h after incubation with Wm (33 μM). Bar, 10 μm (*D*). (*E*) The signal intensity ratio of internalized vs. PM PIN2:GFP as shown in *D* (n = 75 to 90 cells from 15 to 18 seedlings). Data represent mean ± SE with different letters to denote significant differences in one-way ANOVA with Tukey's unequal N-HSD post hoc test, $P < 0.05$; *C*, *E*). (*F*) A hypothetical model illustrating that the phosphorylation status of PIN-HL affects the interaction between PIN-HL and FAB1C and alters the trafficking destination of PIN. Circled numbers in the endosomal membrane depict PtdIns. N and C in PIN indicate N and C terminus, respectively.

protein pulldown assays. Single or double phospho-mutated S1~3 and S5 did not or only marginally affected the interaction of PIN2-HL with FAB1C-N (*SI Appendix*, Fig. S10 *A* and *B*). However, the interaction between PIN2-HL and FAB1C-N was significantly compromised by the phospho-mimetic triple mutation of S1~3 (S1/2/3D) or the M3 phospho-mimetic mutation (M3D) of PIN2-HL (Fig. 4*A*). In contrast, the interaction affinities of the phospho-defective versions of PIN2-HL (S1/2/3A and M3A) with FAB1C-N were similar to that of the unphosphorylated WT-PIN2 in this in vitro phosphorylation assay system (Fig. 4*A*). These phospho-sites in PIN2-HL were also required for the interaction with FAB1B-N (*SI Appendix*, Fig. S10*C*). These results suggest that the phosphorylation status of these sites in PIN2-HL can modulate the interaction with FAB1C and its homologs. However, the phosphorylation residues of PIN-HL are not likely to directly interact with the PIN-interacting module (PD) of FAB1C. The PIN-HL phosphorylation sites affecting the interaction between FAB1C and PIN2-HL (i.e., S1~3, and M3) are located in the HL1 and HL2 regions (*SI Appendix*, Fig. S2), whereas FAB1C preferably interacted with the HL3 region (Fig. 1*C*). This suggests that the phosphorylation sites in HL1 and HL2 could indirectly influence the interaction, possibly by remotely modifying the structure of

the HL3 region, or by recruiting adaptor molecules that mediate the interaction between PIN2-HL and FAB1C.

The finding that unphosphorylated PIN2 has a higher affinity for FAB1C than phosphorylated PIN2 suggests that unphosphorylated PIN2 may be more susceptible to FAB1C-mediated vacuolar trafficking. To test this hypothesis, we compared the vacuolar trafficking of three transgenic constructs: WT-, M3A-, and M3E-PIN2 in the *pin2* mutant background. After an 8-h dark period, the vacuolar trafficking of M3A-PIN2 was 83% higher than that of WT-PIN2, while M3E-PIN2 displayed a level of vacuolar trafficking similar to WT-PIN2. These results suggest that unphosphorylated PIN2 is more likely to be trafficked to the vacuole than its phosphorylated counterpart. In a further test, wortmannin, a PtdInsP3-kinase inhibitor, was used. Wortmannin is known to block the endocytic trafficking of PIN proteins to the vacuole, causing the accumulation of PIN-including wortmannin bodies (15, 24, 56). We hypothesized that proteins more actively involved in vacuolar trafficking would form more wortmannin bodies than less active proteins. Indeed, the formation of wortmannin bodies followed the order M3A-PIN2 > WT-PIN2 > M3E-PIN2 (Fig. 4 *D* and *E*), supporting the idea that unphosphorylated PIN2 is more prone to vacuolar trafficking than phosphorylated PIN2 (Fig. 4*F*).

FAB1C Is Involved in Lateral Root Development and Other Biological Processes. Because FAB1C modulates PIN trafficking, we examined its role in auxin-related biological processes with its loss-of-function mutant, transgenic lines complemented with WT- or mutated-FAB1C, and overexpression lines. First, we focused on the lateral root formation as *FAB1C* was highly expressed during lateral root formation (*SI Appendix*, Fig. S4*C*). In the *fab1c* mutant, lateral root density was up to 26% higher compared to WT, while the growth of the primary root was not significantly different (Fig. 5*A* and *SI Appendix*, Fig. S11 *A* and *C–E*). In addition, we observed whether other FAB1 homologs are also involved in lateral root formation. The lateral root density was not affected in the *fab1b* or *fab1d* single mutant or the *fab1b/fab1d* double mutant, but *fab1b/fab1c* and *fab1c/fab1d* double mutants showed similar levels of lateral root density as the *fab1c* single mutant (Fig. 5*A*). This indicates that among the tested FAB1s, FAB1C is specifically involved in lateral root development.

Next, we assessed the lateral root phenotypes of *FAB1C*-overexpressing lines, along with the *fab1c* mutant complemented with either WT or mutated FAB1C in its PD or PIK domain. The mutant complemented with WT-FAB1C (*ProFAB1C:FAB1C:GFP*) exhibited a restoration to WT-level lateral root density, whereas the FAB1C-overexpressing lines (*Pro35S:FAB1C:RFP*) maintained only 62% of lateral root density compared to WT (Fig. 5*B*). This suggests that FAB1C plays a negative role in lateral root formation. In contrast, *fab1c* mutants complemented with either ΔPD-FAB1C or mPIK-FAB1C were unable to restore WT-level lateral root density while their *FAB1C* transcript levels were similar to that of WT-*FAB1C* (Fig. 5*B* and *SI Appendix*, Fig. S11*B*), implying that both the interaction with PIN and the PtdIns-kinase activity are essential for FAB1C's role in lateral root development.

We then investigated the impact of altered PIN1 polarity and auxin maxima formation, both critical factors in lateral root development (57), by examining auxin levels and PIN1 polarity in both WT and the *fab1c* mutant. Regarding auxin-sensitive DR5 promoter activity, the *fab1c* mutant exhibited higher auxin levels in lateral root primordia, aligning with the mutant's increased lateral root density (Fig. 5 *C* and *D*). However, there was no noticeable difference in auxin levels in the primary root meristem between WT and the mutant (*SI Appendix*, Fig. S11 *F* and *G*), suggesting FAB1C's specific function in the lateral root. The periclinal (outer lateral) PIN1 polarity, known for its importance in auxin transport toward developing lateral root primordia (57), was also assessed. When comparing PIN1 protein levels in the PM of developing lateral root primordial cells between WT and the *fab1c* mutant, although the overall PIN1 intensity increased in the mutant, the PIN1 intensity at the periclinal PM was significantly higher in the *fab1c* mutant than in WT (Fig. 5 *E* and *F*). This may enhance auxin transport toward developing lateral root primordia in the mutant. To understand the increased PIN1 protein level in the mutant, we compared PIN1 transcript and protein levels in *ProPIN1:PIN1:GFP*-containing WT and *fab1c* mutant plants. Despite lower PIN1 transcript levels in the *fab1c*-background transgenic lines used for observation, the PIN1 protein level was higher in the *fab1c* mutant than in WT (Fig. 5*G*). This is likely due to decreased vacuolar trafficking of the PIN1 protein in the *fab1c* mutant.

Given that cytokinin inhibits lateral root formation (29), and that cytokinin-induced vacuolar PIN1 accumulation was reduced in the lateral root primordial cells of the *fab1c* mutant (Fig. 3 *E* and *F*), we hypothesized that the cytokinin-inhibited lateral root formation might be restored in the *fab1c* mutant. In the presence of BA (0.1 μM), lateral root formation was almost completely suppressed in WT, but partially restored in the *fab1c* mutant (Fig. 5 *H* and *I*). The efficacy of BA-mediated lateral root inhibition was approximately 24% less in the absence of *FAB1C* (Fig. 5*J*). This suggests that cytokinin-induced PIN1 degradation and lateral root inhibition partially depend on FAB1C-mediated vacuolar trafficking of PIN1.

Besides lateral root phenotypes, the *fab1c* mutant exhibited a minor defect in root gravitropism. This was rectified by reintroducing WT-FAB1C into the mutant, which restored the WT phenotype (*SI Appendix*, Fig. S12*A*). This minor root gravitropism phenotype of the *fab1c* mutant could be due to functional redundancy among FAB1 homologs in the root. Noting that FAB1C was highly expressed in the hydathode region (*SI Appendix*, Fig. S4*A*), we investigated FAB1C's role in leaf-margin morphogenesis. We observed in the leaf serrations that both the number and height of teeth were marginally increased in the *fab1c* mutant as compared to WT (*SI Appendix*, Fig. S12 *B–D*). Prior research has implicated PIN1 in creating local auxin maxima at the serration teeth (58). Given these findings, we propose that FAB1C might participate in various biological processes where PIN proteins mediate the formation of local auxin gradients.

Discussion

The mechanism by which cargos identify their target destination during endomembrane trafficking is a fascinating question in eukaryotic cellular processes. One logical hypothesis is that the cargo itself possesses specific molecular cues that reader proteins can recognize, consequently determining the trafficking pathway to a particular destination. While such reader proteins have typically been identified as adaptor proteins within the trafficking complex (59), our study introduces the lipid-modifying enzyme PtdIns(3)P5-kinase as a potential cargo reader and effector.

The phosphorylation status at the inositol head of PtdIns sequentially alters across the transforming endomembrane compartments during endocytic and lytic pathways. In this process, PtdIns(3)P5-kinase (FAB1)-mediated phosphorylation of PtdIns(3)P to PtdIns(3,5) P_2 is a distinctive feature during the transition from EE to LE/PVC/MVB (33, 34, 60, 61). Although scarcely reported in other eukaryotic organisms, several plant studies suggest FAB1's involvement in lytic cargo trafficking. Diminished FAB1A/B expression or FAB1 inhibitor treatment impairs the

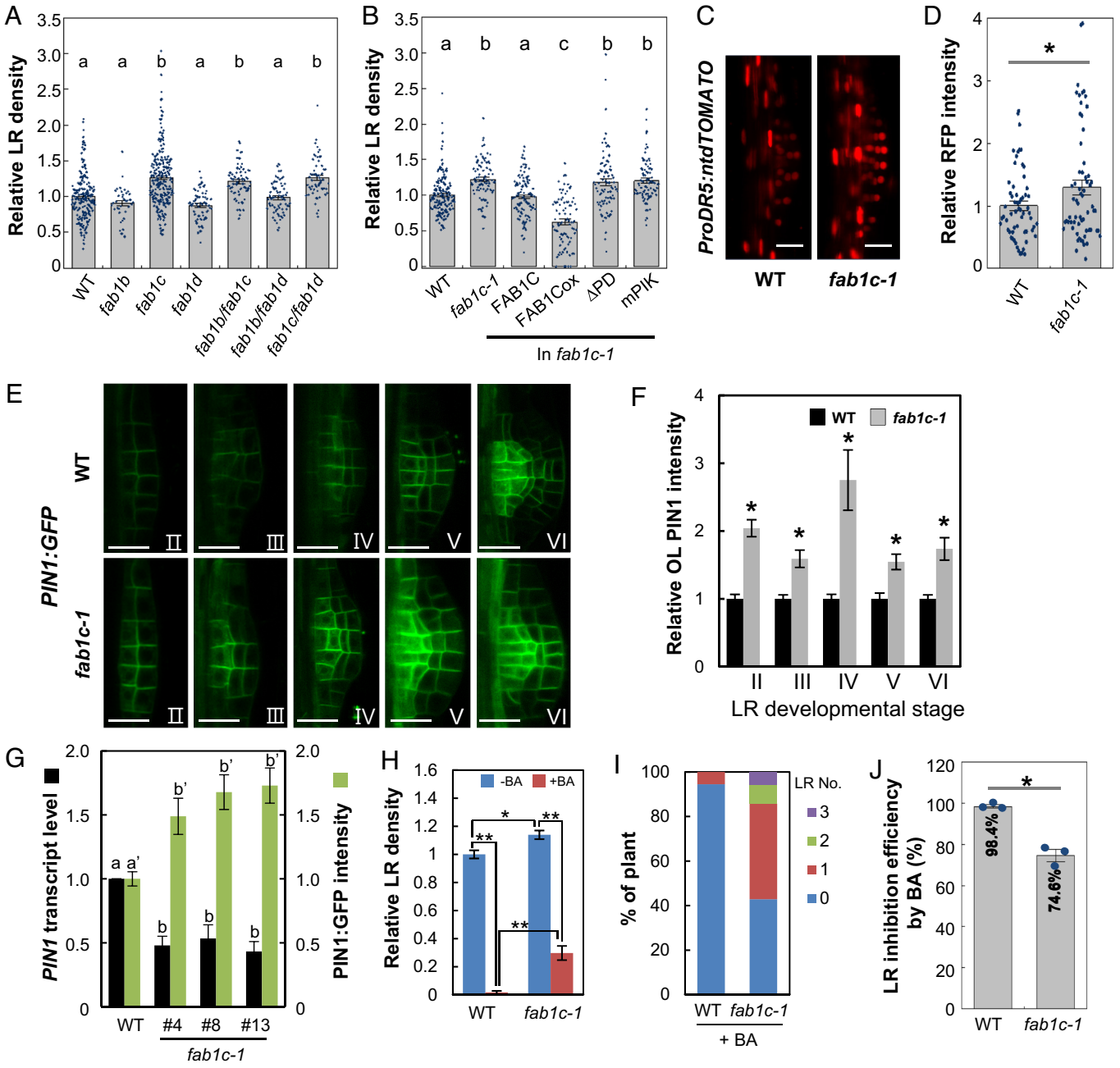

Fig. 5. The role of FAB1C in lateral root development. (*A*) Relative lateral root (LR) densities (number of emerged LRs per cm of the root) in WT and *fab1* mutants backgrounds (n = 36 to 222 seedlings). (*B*) Relative LR densities of WT, *fab1c-1, ProFAB1C:FAB1C:GFP* in *fab1c-1* (FAB1C), *Pro35S:FAB1C:RFP* in WT (FAB1Cox), and *fab1c-1* complemented with mutated FAB1C as described in Fig. 1*F* (n = 83 to 158 seedlings from six independent lines per construct). (*C*) Confocal images of *ProDR5:ntdTOMATO* in the LR primordia of WT and *fab1c-1*. (Bar, 20 μm.) (*D*) Quantification of *ProDR5:ntdTOMATO* expression as shown in *C*. (*E*) Confocal images showing subcellular localization of PIN1 (*ProPIN1:PIN1:GFP*) in developing LR primordia. (Bar, 10 μm.) (*F*) Relative PIN1:GFP intensity at the outer lateral (OL) PM (n = 5 to 19 LR-emerging regions, 8 to 15 seedlings). Roman numbers denote different developmental stages of LR primordia (*E* and *F*). (*G*) Expression analysis of *PIN1:GFP* in WT and *fab1c-1*. Nine-day-old seedlings were analyzed for qRT-PCR of *PIN1* transcript and observation of the PIN1:GFP intensity in LR primordia. (*H–J*) Cytokinin (BA, 0.1 μM) effect on the LR density of WT and *fab1c-1*. (*H*) Relative density of emerged LR. (*I*) Percentage of seedlings including different LR numbers (No.). (*J*) The efficacy of LR inhibition by cytokinin (% of [LR density without BA – LR density with BA]/LR density without BA); n = 3 independent experiments with 35 to 36 seedlings (*H–J*). Data represent mean ± SE, and significant differences are denoted by * (*D*, *F*, *H*, and *J*; Student's *t* test, $*P < 0.05$ $**P < 0.0001$) and different letters (*A*, *B*, and *G*; one-way ANOVA with Tukey's unequal N-HSD post hoc test, $P < 0.05$).

vacuolar trafficking of FM4-64 dye (40, 42) and the vacuolar lytic process of PIN2 (41). FAB1 inhibitor treatment also inhibits the borate-induced vacuolar degradation of the BOR1 borate transporter (42). However, the mechanism by which FAB1 mediates this lytic cargo trafficking remains unclear. Our results suggest that FAB1C, an Arabidopsis PtdIns(3)P5-kinase, serves as an intimate modulator for the vacuolar trafficking of PIN cargos.

What stands out most in this FAB1C-mediated PIN lytic trafficking is the direct interaction of FAB1C with PIN cargos (Figs. 1, 3 *G* and *H*, and 4 and *SI Appendix*, Fig. S10). Canonical FAB1s with the FYVE domain can be recruited to the target endosome by recognizing PtdIns(3)P on it, resulting in PtdIns(3,5) P_2 production and cargo trafficking from those endosomes to the vacuole/lysosome (41, 62). In this process, a physical interaction between PtdIns(3)P5-kinase and cargo appears not to be essential

for simply directing the cargo to a lytic pathway; generating PtdIns(3,5) P_2 could be sufficient to recruit downstream effectors for lytic trafficking (63, 64, 65). However, it was unclear how noncanonical FAB1s such as FAB1C and FAB1D, which lack the FYVE domain, perform equivalent molecular and cellular functions to those of canonical FAB1s (39, 45; our study). Our results demonstrated that FAB1C directly interacted with PIN-HL (Fig. 1), and the absence of the PIN-interacting domain of FAB1C led to the failure of PIN2's lytic trafficking (Fig. 3 *G* and *H*). These findings support the idea that physical interaction with cargo could provide FAB1C with a molecular cue for targeting the cargo-carrying endomembrane to produce PtdIns(3,5)P_2 and initiate lytic trafficking (Fig. 4*F*). Our results showed that canonical FAB1s (FAB1A and FAB1B) were also capable of interacting with PIN2-HL (Fig. 1*D*), suggesting that the recognition of PIN cargo can be generalized among FAB1 homologs. For canonical FAB1s, it is conceivable that interaction with cargo might simply provide them with cargo specificity.

Another significant aspect of the interaction between FAB1C and PIN cargo is that the phosphorylation status of PIN-HL modulates this interaction. The cytosolic HL domain of long PINs includes multiple phosphorylation sites that are phosphorylated by various protein kinases (43, 53). These HL phosphorylation sites serve as key regulatory cues for PIN trafficking and activity. However, it is unknown how this HL phosphorylation status influences PIN behavior. In particular, the phosphorylation status of PIN-HL has been implicated in PIN lytic processes. Phospho-defective PIN3 was more likely to traffic to the vacuole in root hair cells (15), and phospho-mimetic PIN1 was less sensitive to cytokinin-triggered PIN1 degradation than phospho-defective PIN1 in lateral root primordial cells (30). Our findings reveal that the PIN-HL phosphorylation status influences PIN's interaction with FAB1C and FAB1C-mediated lytic trafficking of PINs; namely, unphosphorylated PIN forms have a higher affinity to FAB1C and are more prone to lytic trafficking than phosphorylated PIN forms (Fig. 4).

The polarity of PIN1, PIN2, and PIN3 in the PM was compromised in *fab1c* mutants when compared to WT (Fig. 2 *C*, *H*, and *M* and *SI Appendix*, Fig. S6 *C* and *H*), indicating that the lytic trafficking of PIN is required for maintaining intact PIN polarity. Considering that unphosphorylated PIN2, which has a higher affinity for FAB1C, is more likely to undergo lytic trafficking than phosphorylated PIN2 (Fig. 4), we propose that unphosphorylated PIN exhibits reduced polarity, and that the increased vulnerability of unphosphorylated PIN to lytic trafficking by FAB1C could lead to more intact PIN polarity. Previous studies have demonstrated that unphosphorylated PIN forms display compromised polarity. Phospho-defective mutations of PIN1 at M3 sites or Ca^{2+}-dependent Protein Kinase 29 (CPK29) target sites, along with mutations at M3 sites or Canalization-related Auxin-regulated Malectin-type RLK (CAMEL) target sites, weakened the basal and the basal/inner lateral polarity of PIN1, respectively in vascular cells and endodermal cells of the root (43, 55, 66). Moreover, phospho-defective mutations of PIN2 at CPK29 target sites decreased the apical polarity in root epidermal cells (43), and phospho-defective mutations of PIN3 at M3 sites also compromised its basal and inner lateral polarity (15). Taken together, these observations support the hypothesis that FAB1C may sharpen the polarity of PINs by promoting the removal of less polar, unphosphorylated PINs.

FAB1s exhibit a variety of subcellular localizations. FAB1A primarily localizes to LEs in root tissues (41) and to the PM of a growing root hair shank (46). FAB1B localizes to ER-like structures and vacuoles in pollen tubes (45). In contrast, noncanonical FAB1C and FAB1D are mainly localized in the cytoplasm (45; *SI Appendix*, Fig. S4 *B* and *C* in this study). Despite the diversity in subcellular localization, FAB1 homologs appear to share biological functions. FAB1A and FAB1B are functionally redundant for pollen viability in Arabidopsis (38). Notably, even cytoplasm-localized noncanonical FAB1s displayed functional redundancy with canonical FAB1s. Both FAB1B and FAB1D are involved in the regulation of membrane recycling, vacuolar pH, and the homeostatic production of reactive oxygen species (ROS) in pollen tubes (45), and FAB1B and FAB1C played a similar role in stomatal movement in Arabidopsis (39). The redundancy of biological functions among FAB1 homologs, regardless of the presence of the FYVE domain, suggests that their molecular and cellular functions would be essentially compatible with each other. Conversely, our results demonstrate that this functional compatibility among FAB1s could operate in a spatiotemporal context. It was previously reported that both the suppression of FAB1A and FAB1B or the overexpression of FAB1A did not affect lateral root formation (40). However, our results showed that the loss of FAB1C enhanced and its overexpression inhibited lateral root formation, while the loss of both FAB1B and FAB1D did not affect lateral root formation (Fig. 5 *A* and *B*). This functional discrepancy does not seem to be simply due to the tissue-specific expression issue among FAB1s because all FAB1 homologs show considerable expression levels in lateral root primordia, though the FAB1C expression level was higher than those of other homologs (67). These results together also suggest the possibility of functional diversification among FAB1s.

While our study reports the direct interaction between FAB1 and PINs, it should be further explored whether this FAB1-cargo interaction is general for other cargos destined for lytic trafficking. Additionally, an important question for future research is how the FAB1 product, PtdIns(3,5)P_2, facilitates lytic trafficking.

Materials and Methods

Plant Materials and Growth Conditions. *Arabidopsis thaliana* Columbia ecotype (Col-0) plants were used as WT and for transformation with transgene constructs. The *fab1c-3* mutant was obtained from the Arabidopsis Stock Center (https://www.Arabidopsis.org/). The *fab1a, fab1b, fab1c-1,* and *fab1d* mutant seeds were provided by Youngsook Lee (Pohang University). Multiple mutants were generated by crossing individual lines, and their homozygosity was confirmed by PCR. Seeds were treated at 4 °C for 4 d before germination and cultivation at 22 °C under a 16-h light/8-h dark photoperiod under fluorescent illumination (FHF 32SS-EXD; Kumho Electric) with a light intensity of 130 μmol m^{-2} s^{-1}. Seedlings were grown on agar plates containing 2.15 g L^{-1} Murashige and Skoog (1/2× MS) nutrient mix (Duchefa, the Netherlands), 1% sucrose, 0.5 g L^{-1} MES (pH 5.7 with KOH), and 0.8% agarose (SeaKem, Cambrex BioScience Rockland). Arabidopsis plants were transformed by the floral dip method using *Agrobacterium tumefaciens* strain C58C1, and transformants were selected on agar plates containing hygromycin (30 μg mL^{-1}) or phosphinothricin (30 μg mL^{-1}) and cefotaxime (10 μg mL^{-1}). Multiple (three to eight) independent transgenic lines and 4-d-old seedlings were analyzed unless stated otherwise.

Transgene Construction. The information about transgene construction is available in *SI Appendix, Materials and Methods*.

Bacterial Protein Expression and In Vitro Protein Pulldown Assays. Plasmids were transformed into *Escherichia coli* BL21-DE3 Rosetta competent cells (Novagen), and protein expression was induced with 1 mM isopropyl β-D-1-thiogalactopyranoside (IPTG) for 4 h. Cells were lysed with Thermo Scientific Pierce B-PER Bacterial Protein Extraction Reagents, comprising 1 mL B-Per, 2 μL DNase1 (5 units μL^{-1}), 20 μL lysozyme (10 mg mL^{-1}), and 1× protease inhibitor cocktail (Roche).

FAB1C, as a PIN-interacting protein (PIP), was identified by using protein pulldown with PIN3-HL as bait and following mass spectrometry analysis as previously described (43).

For in vitro pulldown experiments between FAB1 and PIN-HL, His-tagged FAB1 (His:FAB1) and GST:PIN-HL were expressed in the bacterial cells. Fifty microliter glutathione sepharose beads 4B (GE Lifesciences) were incubated first with ~10 μg GST or GST:PINs-HL for 3 h at 4 °C on a rotator (15 rpm) to allow binding. After removing the supernatant, the beads were incubated with ~10 μg His:FAB1 protein for 2 h at 4 °C on a rotator (15 rpm) for interaction. The beads were then washed five times with 1× Tris-buffered saline (TBS, including 0.1 % [v/v] Tween-20) to remove nonspecifically bound proteins. Bound proteins were isolated from the beads by adding 1× SDS loading dye, separated by SDS-PAGE, transferred to 0.45-μm nitrocellulose membranes (GE Lifesciences), and probed with 1:3,000 diluted anti-His (MBL, cat. # D291-3) and anti-GST antibodies (Abcam, cat. # AB3416). Chemiluminescence detection was performed with the ECL (LPS solution) protein gel-blotting substrate in a chemiluminescence imaging system (Davinch-chem).

Y2H Assays. Y2H assay was performed using the Matchmaker Yeast Two-Hybrid System (Clontech) following the manufacturer's manual. Yeast strain AH109 was used for transformation, and transformed yeast cells were cultured on the SD^{2-} (-Leu and -Trp) plate at 30 °C for 4 d. A single colony was picked and resuspended in the liquid SD^{2-} broth. The yeast suspensions were plated on the SD^{2-} or SD^{3-} (-Leu, -Trp, and -His; including 1 mM 3-amino-1,2,4-triazole) solid medium and incubated at 30 °C for 6 d before observation.

FRET-FLIM Analyses. FRET-FLIM analysis was used to observe the in vivo interaction between FAB1C and PIN2 as previously described (43). Six-day-old seedlings of the double transgenic line containing both *ProPIN2:PIN2:GFP* and *Pro35S:FAB1C:RFP*, which was generated by crossing the two lines, were observed for the FRET-FLIM analysis. Fluorescence confocal imaging and fluorescence lifetime imaging were conducted using an inverted-type scanning confocal microscope (SP8 FALCON, Leica Microsystems) with a 40× (air) objective lens. Picosecond pulsed laser lines (488 and 594 nm) from a white light laser (WLL) system were used as excitation sources. Two hybrid photon detectors (HyD1 & HyD3) were used to collect emissions in the ranges of 495 to 580 nm and 600 to 770 nm from root samples. Fluorescence confocal and lifetime images of 512 × 512 pixels were recorded using a galvo-stage and time-correlated single-photon counting technique. During the imaging, the pinhole was set to 1.0. All data manipulations were performed using the Leica suited software (LAS X Ver.3.5.2). Average lifetime values were calculated by the amplitude-weighted method. The region of interest (ROI) was defined as a rectangular area encompassing the apical PM, intracellular area, or entire epidermal cells within the root-meristem area (*SI Appendix*, Fig. S3*D*).

Histological Observation of β-Glucuronidase (GUS) Activity. GUS expression analysis was performed as described previously (68). Seedlings and other plant parts were incubated in the GUS reaction buffer (1 mM 5-bromo-4-chloro-3-indoyl-β-D-glucuronide cyclohexylammonium salt, 0.1 M NaH_2PO_4, 0.01 M EDTA, 0.1% Triton-X-100, and 0.5 mM potassium ferricyanide pH 7) for 3 h at 37 °C and then destained in 70% ethanol. Images were obtained using an M205 FA stereomicroscope (Leica).

Confocal Microscopic Observations. Observation of fluorescence reporters using a confocal microscope (LSM700, Carl Zeiss) was conducted as described previously (69). Plant seedlings were treated with wortmannin [33 μM from a 20 mM stock solution in dimethyl sulfoxide (DMSO)] or with FM4-64 (2 μM from a 40 mM stock solution in DMSO) in liquid MS medium for given time periods before observation. The dark treatment of seedlings was done on a solid MS medium. For cytokinin (BA) treatment, 7-d-old seedlings were transferred onto the MS medium with or without BA (0.1 μM in 0.05% DMSO) and incubated for 2 h before observation. Controls included an equivalent amount of DMSO. Cell boundary staining was done with propidium iodide (PI, 10 μg mL^{-1}) for 2 min before observation. Quantification of fluorescence signals was performed using ImageJ software.

RNA Isolation and qRT-PCR Analysis. Total RNA was isolated from 4- or 9-d-old seedlings, depending on the experiment, using RNeasy Plant Mini Kit (Qiagen). cDNA was synthesized as described previously (70). qRT-PCR analyses were performed using a SensiFAST SYBR No ROX kit (Bioline) and a CFX connect Real-Time PCR detection system (Bio-Rad). For the semiquantitative RT-PCR analysis between different *FAB1C* variants (*SI Appendix*, Fig. S11*B*), each RNA sample was prepared from six independent lines per construct. Gene-specific signals were normalized to the *ACTIN2* transcript level. Three independent RNA samples were prepared from each plant line, and three technical replicate qRT-PCR reactions were performed for each RNA sample. Primers used for qRT-PCR are listed in *SI Appendix*, Table S1.

Observation of Biological Parameters. Emerged LRs and LR primordia were observed in 9-d-old seedlings. LR number indicates the number of emerged LRs. LR density represented the emerged LR number per cm of the primary root length. For the observation of root gravitropism, root images were taken at the indicated time intervals after 90° gravi-stimulation, and the bending angle was recorded. The number of leaf tooth (serrate) and tooth height were estimated as described in *SI Appendix*, Fig. S12*B*. Four-day-old seedlings were observed to estimate root meristem sizes in terms of the meristem length between the quiescent cell and the cortical cell immediately before the transient zone and the cortical cell number in this meristematic zone.

Statistical Analyses. Statistically significant differences are denoted with different letters (one-way ANOVA with Tukey's unequal N HSD post hoc test, $P < 0.05$) or with asterisks (Student's *t* test as indicated in Figures). Pearson product-moment correlation coefficient (R2) was used to confirm whether the correlation coefficient is significantly different from zero.

Accession Numbers. Sequence data and mutant information are in the Arabidopsis Genome Initiative databases under the following accession numbers: AT4G33240 (*FAB1A*), AT3G14270 (*FAB1B*), AT1G71010 (*FAB1C*), AT1G34260 (*FAB1D*), AT1G73590 (*PIN1*), AT5G57090 (*PIN2*), AT1G70940 (*PIN3*), AT3G187800 (*ACTIN2*), SALK_048293 (*fab1b*), SAIL_254_G09 (*fab1c-1*), SALK_204896C (*fab1c-3*), and SALK_047604 (*fab1d*).

Data, Materials, and Software Availability. All study data are included in the article and/or *SI Appendix*.

ACKNOWLEDGMENTS. We thank Youngsook Lee at Pohang University for the *fab1* mutant seeds. This research was supported by a grant from the National Research Foundation (NRF-2022R1A2C1007862). K.-H.M. and H.L. were partially supported by the Stadelmann-Lee Scholarship Fund at Seoul National University.

Author affiliations: [a]Department of Biological Sciences, Seoul National University, Seoul 08826, South Korea

Author contributions: H.-T.C. designed research; K.-H.M. and H.L. performed research; K.-H.M. and H.-T.C. analyzed data; and K.-H.M. and H.-T.C. wrote the paper.

1. W. Grunewald, J. Friml, The march of the PINs: Developmental plasticity by dynamic polar targeting in plant cells. *EMBO J.* **29**, 2700–2714 (2010).
2. A. Ganguly, D. Sasayama, H.-T. Cho, Regulation of the polarity of protein trafficking by phosphorylation. *Mol. Cells* **33**, 423–430 (2012).
3. P. Křeček *et al.*, The PIN-FORMED (PIN) protein family of auxin transporters. *Genome Biol.* **10**, 249 (2009).
4. J. Friml, J. Wiśniewska, E. Benková, K. Mendgen, K. Palme, Lateral relocation of auxin efflux regulator PIN3 mediates tropism in Arabidopsis. *Nature* **415**, 806–809 (2002).
5. I. Blilou *et al.*, The PIN auxin efflux facilitator network controls growth and patterning in Arabidopsis roots. *Nature* **433**, 39–44 (2005).
6. J. Wiśniewska *et al.*, Polar PIN localization directs auxin flow in plants. *Science* **312**, 883–883 (2006).
7. J. Kleine-Vehn *et al.*, Gravity-induced PIN transcytosis for polarization of auxin fluxes in gravity-sensing root cells. *Proc. Natl Acad. Sci. U.S.A.* **107**, 22344–22349 (2010).
8. Z. Ding *et al.*, Light-mediated polarization of the PIN3 auxin transporter for the phototropic response in Arabidopsis. *Nat. Cell Biol.* **13**, 447–452 (2011).
9. J. Kleine-Vehn *et al.*, Recycling, clustering, and endocytosis jointly maintain PIN auxin carrier polarity at the plasma membrane. *Mol. Syst. Biol.* **7**, 540 (2011).
10. J. Leitner *et al.*, Lysine63-linked ubiquitylation of PIN2 auxin carrier protein governs hormonally controlled adaptation of Arabidopsis root growth. *Proc. Natl Acad. Sci. U.S.A.* **109**, 8322–8327 (2012).
11. M. Zourelidou *et al.*, The polarly localized D6 PROTEIN KINASE is required for efficient auxin transport in Arabidopsis thaliana. *Development* **4**, 627–636 (2009).
12. M. Zourelidou *et al.*, Auxin efflux by PIN-FORMED proteins is activated by two different protein kinases, D6 PROTEIN KINASE and PINOID. *Elife* **3**, e02860 (2014).
13. P. Dhonukshe *et al.*, Plasma membrane-bound AGC3 kinases phosphorylate PIN auxin carriers at TPRXS(N/S) motifs to direct apical PIN recycling. *Development* **13**, 2386–2387 (2010).
14. F. Huang *et al.*, Phosphorylation of conserved PIN motifs directs Arabidopsis PIN1 polarity and auxin transport. *Plant Cell* **22**, 1129–1142 (2010).

15. A. Ganguly, S. H. Lee, H.-T. Cho, Functional identification of the phosphorylation sites of Arabidopsis PIN-FORMED3 for its subcellular localization and biological role. *Plant J.* **71**, 810–823 (2012).
16. I. C. R. Barbosa, M. Zourelidou, B. C. Willige, B. Weller, C. Schwechheimer, D6 PROTEIN KINASE activates auxin transport-dependent growth and PIN-FORMED phosphorylation at the plasma membrane. *Dev. Cell* **29**, 674–685 (2014).
17. K. Haga, L. Frank, T. Kimura, C. Schwechheimer, T. Sakai, Roles of AGCVIII kinases in the hypocotyl phototropism of Arabidopsis seedlings. *Plant Cell Physiol.* **59**, 1060–1071 (2018).
18. B. Weller *et al.*, Dynamic PIN-FORMED auxin efflux carrier phosphorylation at the plasma membrane controls auxin efflux-dependent growth. *Proc. Natl. Acad. Sci. U.S.A.* **114**, E887–E896 (2017).
19. P. Marhava *et al.*, A molecular rheostat adjusts auxin flux to promote root protophloem differentiation. *Nature* **558**, 297–300 (2018).
20. Z. Yang *et al.*, Structural insights into auxin recognition and efflux by Arabidopsis PIN1. *Nature* **7927**, 611–615 (2022).
21. P. Dhonukshe *et al.*, Generation of cell polarity in plants links endocytosis, auxin distribution and cell fate decisions. *Nature* **456**, 962–966 (2008).
22. L. Abas *et al.*, Intracellular trafficking and proteolysis of the Arabidopsis auxin-efflux facilitator PIN2 are involved in root gravitropism. *Nat. Cell Biol.* **8**, 249–256 (2006).
23. Y. Jaillais, I. Fobis-Loisy, C. Miege, C. Rollin, T. Gaude, AtSNX1 defines an endosome for auxin-carrier trafficking in Arabidopsis. *Nature* **443**, 106–109 (2006).
24. J. Kleine-Vehn *et al.*, Differential degradation of PIN2 auxin efflux carrier by retromer-dependent vacuolar targeting. *Proc. Natl Acad. Sci. U.S.A.* **105**, 17812–17817 (2008).
25. R. Whitford *et al.*, GOLVEN secretory peptides regulate auxin carrier turnover during plant gravitropic responses. *Dev. Cell* **22**, 678–685 (2012).
26. P. Baster *et al.*, SCF(TIR1/AFB)-auxin signalling regulates PIN vacuolar trafficking and auxin fluxes during root gravitropism. *EMBO J.* **32**, 260–274 (2013).
27. A. Fernandez *et al.*, Transcriptional and functional classification of the GOLVEN/ROOT GROWTH FACTOR/CLE-like signaling peptides reveals their role in lateral root and hair formation. *Plant Physiol.* **161**, 954–970 (2013).
28. B. Korbei *et al.*, Arabidopsis TOL proteins act as gatekeepers for vacuolar sorting of PIN2 plasma membrane protein. *Curr. Biol.* **23**, 2500–2505 (2013).
29. P. Marhavý *et al.*, Cytokinin modulates endocytic trafficking of PIN1 auxin efflux carrier to control plant organogenesis. *Dev. Cell* **21**, 796–804 (2011).
30. P. Marhavý *et al.*, Cytokinin controls polarity of PIN1-dependent auxin transport during lateral root organogenesis. *Curr. Biol.* **24**, 1031–1037 (2014).
31. N. Jin, M. J. Lang, L. S. Weisman, Phosphatidylinositol 3,5-bisphosphate: Regulation of cellular events in space and time. *Biochem. Soc. Trans.* **44**, 177–184 (2016).
32. M. P. Platre, Y. Jaillais, Guidelines for the use of protein domains in acidic phospholipid imaging. *Methods Mol. Biol.* **1376**, 175–194 (2016).
33. T. Hirano, M. H. Sato, Diverse physiological functions of FAB1 and phosphatidylinositol 3,5-bisphosphate in plants. *Front. Plant Sci.* **10**, 274 (2019).
34. P. J. Cullen, H. C. Korswagen, Sorting nexins provide diversity for retromer-dependent trafficking events. *Nat. Cell Biol.* **14**, 29–37 (2012).
35. S. Schmid, M. Mettlen, Lipid switches and traffic control. *Nature* **499**, 161–162 (2013).
36. A. Shisheva, PIKfyve: Partners, significance, debates and paradoxes. *Cell Biol. Int.* **32**, 591–604 (2008).
37. B. Mueller-Roeber, C. Pical, Inositol phospholipid metabolism in Arabidopsis. Characterized and putative isoforms of inositol phospholipid kinase and phosphoinositide-specific phospholipase C. *Plant Physiol.* **130**, 22–46 (2002).
38. P. Whitley, S. Hinz, J. Doughty, Arabidopsis FAB1/PIKfyve proteins are essential for development of viable pollen. *Plant Physiol.* **151**, 1812–1822 (2009).
39. G. Bak *et al.*, Rapid structural changes and acidification of guard cell vacuoles during stomatal closure require phosphatidylinositol 3,5-bisphosphate. *Plant Cell* **25**, 2202–2216 (2013).
40. T. Hirano, T. Matsuzawa, K. Takegawa, M. H. Sato, Loss-of-function and gain-of-function mutations in FAB1A/B impair endomembrane homeostasis, conferring pleiotropic developmental abnormalities in Arabidopsis. *Plant Physiol.* **155**, 797–807 (2011).
41. T. Hirano, T. Munnik, M. H. Sato, Phosphatidylinositol 3-phosphate 5-kinase, FAB1/PIKfyve kinase mediates endosome maturation to establish endosome-cortical microtubule interaction in Arabidopsis. *Plant Physiol.* **169**, 1961–1974 (2015).
42. T. Hirano, T. Munnik, M. H. Sato, Inhibition of phosphatidylinositol 3,5-bisphosphate production has pleiotropic effects on various membrane trafficking routes in Arabidopsis. *Plant Cell Physiol.* **58**, 120–129 (2017).
43. H. Lee, A. Ganguly, B. Song, H.-T. Cho, Calcium-dependent protein kinase 29 modulates PIN-FORMED polarity and Arabidopsis development via its own phosphorylation code. *Plant Cell* **33**, 3513–3531 (2021).
44. J. D. Gary, A. E. Wurmser, C. J. Bonangelino, L. S. Weisman, S. D. Emr, Fab1p is essential for PtdIns(3) P 5-kinase activity and the maintenance of vacuolar size and membrane homeostasis. *J. Cell Biol.* **143**, 65–79 (1998).
45. S. Serrazina, F. V. Dias, R. Malhó, Characterization of FAB1 phosphatidylinositol kinases in Arabidopsis pollen tube growth and fertilization. *New Phytol.* **203**, 784–793 (2014).
46. T. Hirano *et al.*, PtdIns(3,5)P2 mediates root hair shank hardening in Arabidopsis. *Nat. Plants* **4**, 888–897 (2018).
47. J. M. Gaullier *et al.*, FYVE fingers bind PtdIns(3)P. *Nature* **394**, 432–433 (1998).
48. F. C. Reyes, R. Buono, M. S. Otegui, Plant endosomal trafficking pathways. *Curr. Opin. Plant Biol.* **14**, 666–673 (2011).
49. T. Ueda, T. Uemura, M. H. Sato, A. Nakano, Functional differentiation of endosomes in Arabidopsis cells. *Plant J.* **40**, 783–789 (2004).
50. J. Dettmer, A. Hong-Hermesdorf, Y.-D. Stierhof, K. Schumacher, Vacuolar H^+-ATPase activity is required for endocytic and secretory trafficking in Arabidopsis. *Plant Cell* **18**, 715–730 (2006).
51. R. Tejos, C. Osorio-Navarro, L. Norambuena, The use of drugs in the study of vacuole morphology and trafficking to the vacuole in *Arabidopsis thaliana*. *Methods Mol. Biol.* **1789**, 143–154 (2018).
52. A. Laxmi, J. Pan, M. Morsy, R. Chen, Light plays an essential role in intracellular distribution of auxin efflux carrier PIN2 in *Arabidopsis thaliana*. *PLoS One* **3**, e1510 (2008).
53. U. Z. Hammes, A. S. Murphy, C. Schwechheimer, Auxin transporters-A biochemical view. *Cold Spring Harb. Perspect. Biol.* **2**, a039875 (2022).
54. D. Sasayama, A. Ganguly, M. Park, H.-T. Cho, The M3 phosphorylation motif has been functionally conserved for intracellular trafficking of long-looped PIN-FORMEDs in the Arabidopsis root hair cell. *BMC Plant Biol.* **13**, 189 (2013).
55. D. Ki, D. Sasayama, H.-T. Cho, The M3 phosphorylation site is required for trafficking and biological roles of PIN-FORMED1, 2, and 7 in Arabidopsis. *Front. Plant Sci.* **7**, 1479 (2016).
56. M. Cho, J. Lee, H.-T. Cho, ATP-Binding Cassette B4, an auxin-efflux transporter, stably associates with the plasma membrane and shows distinctive intracellular trafficking from that of PIN-FORMEDs. *Plant Physiol.* **159**, 642–654 (2012).
57. E. Benková *et al.*, Local, efflux-dependent auxin gradients as a common module for plant organ formation. *Cell* **115**, 591–602 (2003).
58. G. D. Bilsborough *et al.*, Model for the regulation of Arabidopsis thaliana leaf margin development. *Proc. Natl Acad. Sci. U.S.A.* **108**, 3424–3429 (2011).
59. D. Arora, D. Van Damme, Motif-based endomembrane trafficking. *Plant Physiol.* **186**, 221–238 (2021).
60. I. Heilmann, Phosphoinositide signaling in plant development. *Development* **143**, 2044–2055 (2016).
61. T. Hirano, K. Stecker, T. Munnik, H. Xu, M. H. Sato, Visualization of phosphatidylinositol 3,5-bisphosphate dynamics by a tandem ML1N-based fluorescent protein probe in Arabidopsis. *Plant Cell Physiol.* **58**, 1185–1195 (2017).
62. M. A. Lemmon, Membrane recognition by phospholipid-binding domains. *Nat. Rev. Mol. Cell Biol.* **9**, 99–111 (2008).
63. C. Stroupe, K. M. Collins, R. A. Fratti, W. Wickner, Purification of active HOPS complex reveals its affinities for phosphoinositides and the SNARE Vam7p. *EMBO J.* **25**, 1579–1589 (2006).
64. C. Brillada *et al.*, Phosphoinositides control the localization of HOPS subunit VPS41, which together with VPS33 mediates vacuole fusion in plants. *Proc. Natl Acad. Sci. U.S.A.* **115**, E8305–E8314 (2018).
65. F. Aniento, V. S. M. Hernández, Y. Dagdas, M. Rojas-Pierce, E. Russinova, Molecular mechanisms of endomembrane trafficking in plants. *Plant Cell* **34**, 146–173 (2022).
66. J. Hajný *et al.*, Receptor kinase module targets PIN-dependent auxin transport during canalization. *Science* **6516**, 550–557 (2020).
67. S. M. Brady *et al.*, A high-resolution root spatiotemporal map reveals dominant expression patterns. *Science* **5851**, 801–806 (2007).
68. H.-T. Cho, D. J. Cosgrove, Altered expression of expansin modulates leaf growth and pedicel abscission in Arabidopsis thaliana. *Proc. Natl Acad. Sci. U.S.A.* **17**, 9783–9788 (2000).
69. A. Ganguly *et al.*, Differential auxin-transporting activities of PIN-FORMED proteins in Arabidopsis root hair cells. *Plant Physiol.* **153**, 1046–1061 (2010).
70. S. H. Lee, H.-T. Cho, PINOID positively regulates auxin efflux in Arabidopsis root hair cells and tobacco cells. *Plant Cell* **18**, 1604–1616 (2006).